

The Open University's repository of research publications
and other research outputs

Residual stress control of multipass welds using low transformation temperature fillers

Journal Item

How to cite:

Moat, R. J.; Ooi, S.; Shirzadi, A. A.; Dai, H.; Mark, A. F.; Bhadeshia, H. K. D. H. and Withers, P. J. (2018). Residual stress control of multipass welds using low transformation temperature fillers. *Materials Science and Technology*, 34(5) pp. 519–528.

For guidance on citations see [FAQs](#).

© 2017 Institute of Materials, Minerals and Mining

Version: Accepted Manuscript

Link(s) to article on publisher's website:

<http://dx.doi.org/doi:10.1080/02670836.2017.1410954>

Copyright and Moral Rights for the articles on this site are retained by the individual authors and/or other copyright owners. For more information on Open Research Online's data [policy](#) on reuse of materials please consult the policies page.

Residual stress control of multipass welds using low transformation temperature fillers

R.J. Moat^{1,2*}, S. Ooi³, A.A. Shirzadi², H. Dai¹, A.F. Mark¹, H.K.D.H. Bhadeshia³ and P.J.

Withers⁴

1 formally at School of Materials, University of Manchester, Manchester, M13 9PL, UK

2 Materials Engineering, Open University, Milton Keynes, MK12 6AA, UK

3 Department of materials, University of Cambridge, Cambridge, CB2 4MS, UK

4 School of Materials, University of Manchester, Manchester, M13 9PL, UK

* Corresponding Author: Richard.Moat@open.ac.uk

Abstract

Low transformation temperature (LTT) weld fillers can be used to control residual stresses and distortion of single pass welds in austenitic plates. By contrast, weld fillers in multipass welds experience a number of thermal excursions, meaning that the benefit of the smart LTT fillers may not be realised. Here neutron diffraction and the contour method are used to measure the residual stress in an 8 pass groove weld of a 304L stainless steel plate using the experimental LTT filler Camalloy 4. Measurements show that the stress mitigating effect of Camalloy 4 is indeed diminished during multipass welding and the use of carefully selected elevated interpass hold temperature restores the LTT capability to successfully mitigate residual tensile stresses.

Martensitic transformation; gas metal arc welding; displacive transformation; low stress low distortion welding;

Introduction

Tensile residual stresses that form as a result of welding can have a deleterious effect on the structural integrity, leading to component distortion, mechanical under performance, or even catastrophic failures [1]. Such stresses can be especially problematic for the nuclear power industry [2], because there are many thick and large welded sections which cannot be heat treated to reduce residual stresses. Further, in pressurised water reactor (PWR) assemblies, such welds can experience operating conditions which increase their susceptibility to “environmentally assisted cracking” (EAC) or creep cavitation [3], both of which

are strongly affected by residual stresses. This makes control and mitigation of residual stress in welded joints an important feature of modern weld design.

An elegant and efficient method of residual stress mitigation, exploiting transformation plasticity associated with the martensitic transformation in ferritic steel, was shown by Wang et al. [4] and Ohta et al. [5] to be highly effective. This approach requires a sufficiently low martensite start temperature, M_s , of the filler material. However these early studies tended to rely on the martensitic transformation resulting in welds with impractically low toughness. The focus was therefore shifted to the design of low transformation temperature (M_s) weld fillers with higher toughness, both for stainless steels [6] and ferritic steels [7–9]. In these studies, alloys specially designed to have low M_s and good mechanical properties were selected, for which suitable alloy design processes are reported in [6]. The ability to control the state of residual stress using such alloys has been demonstrated by Dai et al. [10], Murakawa et al. [11], Moat et al. [12], Thibault et al. [13] Dixneit et al. [14,15] and Ramjaun et al. [8,9,16] who used neutron diffraction, x-ray diffraction and/or the contour method to quantify the residual stresses. Further, these stresses have been well explained by finite element models that capture the transformation strain along with associated transformation plasticity [17,18].

The low transformation temperature filler reported by Shirzadi et al. in [6], named Camalloy 4, is a martensitic stainless steel. As is evident from the Satoh test shown in Figure 1 it has a martensite start temperature, M_s of approximately 200°C. This, alongside good mechanical properties, makes it well suited as a stress mitigating filler material for the welding of austenitic stainless steel; giving high strength, high toughness and low distortion welds. To date only single pass welds of Camalloy 4 have been examined [12].

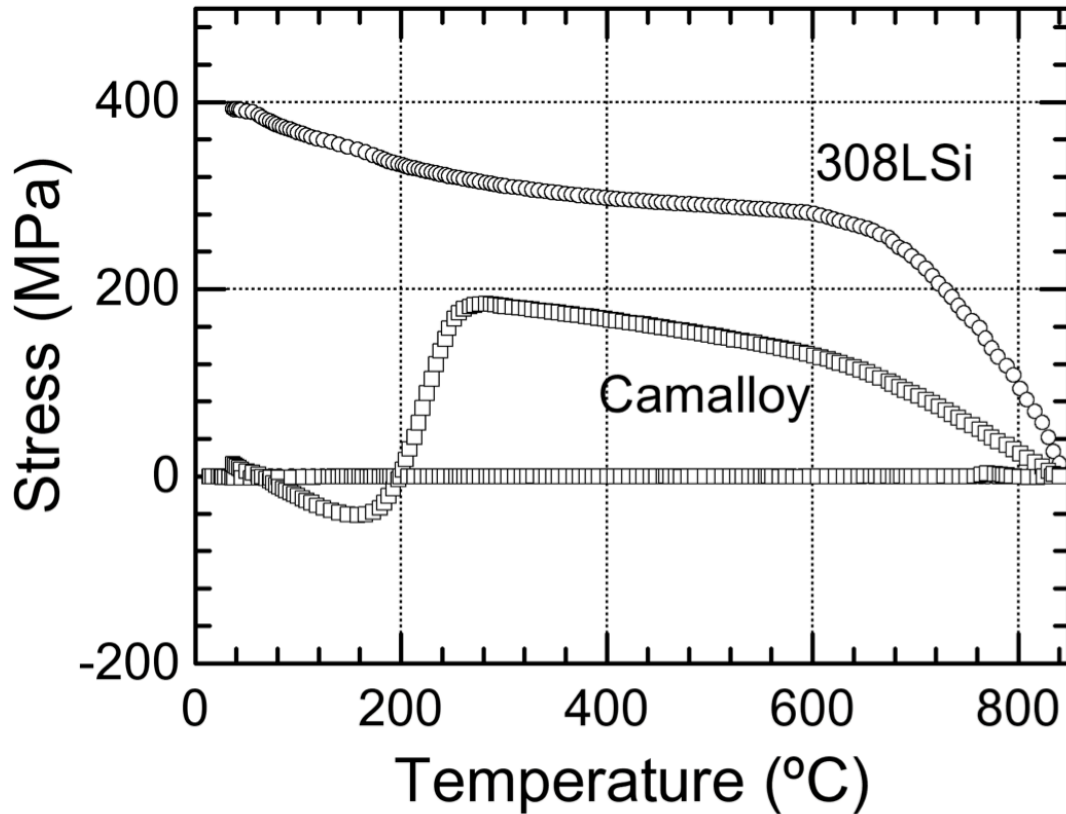


Figure 1: Stress recorded during constrained cooling (Sato test) of the two filler metals used in this study [12].

Since single pass welds undergo only one thermal excursion the transformation upon cooling is relatively easy to control. By contrast the weld filler in multipass welds experiences several thermal excursions of decreasing intensity as subsequent weld passes are applied. This opens up the possibility of tensile residual stresses being generated in a multipass weld upon subsequent reheating cycles that are sufficient to cause re-austenisation of the already deposited layers but are not cooled sufficiently to regenerate martensitic structure. In this paper control of interpass temperature is investigated as a means of maintaining entire weld in an austenitic state until welding is completed. The subsequent martensitic transformation of the multipass weld would then compensate for the thermal contraction to yield a favourable residual stress distribution.

Experimental

Material and weld preparation

Four identical plates (200 × 150 × 20 mm) were prepared from conventional austenitic stainless steel (304L). A half-thickness deep, V-groove was machined along the centreline of each plate, with an enclosed angle of 60°. The thermal history was followed during welding by thermocouples spot-welded onto the surface of the plate near the groove. The preparation of the plate for welding, the order of weld beads and its representation in FE are shown in Figure 2. The plate was restrained by fillet welds to the work bench (tack welded) on all sides of the plate.

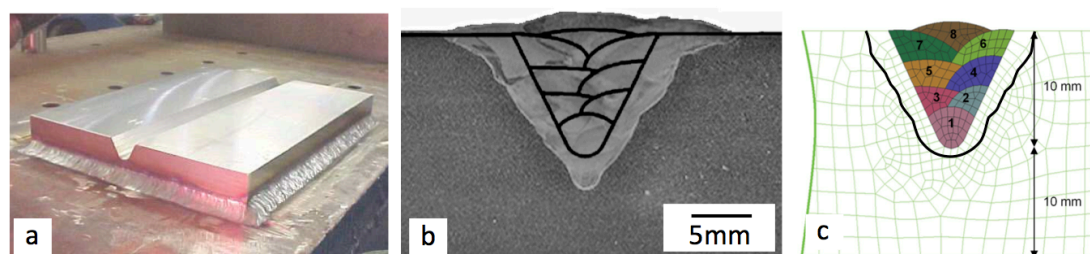


Figure 2: a) A photograph of the grooved plates prepped for welding, b) optical macrograph showing the fusion zone and the weld lay-up sequence for the gas metal arc welds, c) finite element mesh used in the multipass weld model showing each pass and the 1500°C thermal contour that approximates to the fusion zone boundary.

Two filler metals were chosen; the first, CamAlloy 4, designed to have corrosion resistance as well as a low transformation temperature [6]; the second, Autorod 308LSi, which is a commercially available non-transforming austenitic filler metal commonly used for welding 304L steel. The chemical compositions of CamAlloy 4, Autorod 308LSi and 304L base metal are listed in Table 1.

Table 1: Chemical compositions (wt%).

Alloys	C	Si	Cr	Ni	Mo	N	Mn
CamAlloy 4	0.01	0.73	13.00	6.00	0.06	0.026	1.50
Autorod OK 308LSi	0.01	0.90	19.70	10.70	0.00	0.01	1.90
304L (base)	0.03	0.75	18.00	8.00	0.00	0.10	2.00

The weld trials were carried out using gas metal arc welding with a shielding gas of 98%Ar-2%CO₂. The welding current and voltage were 230-295 A and 26-30 V,

respectively, and the welding speed was between 65-78 mm min⁻¹. Eight layers of filler metal were deposited on each plate using the interpass hold temperatures given in Table 2. Plate T50 and plate T200 are produced to investigate the effect of inter-pass temperature; while plate A50 serves as a reference to current industry practice.

Table 2: Summary of welding conditions.

Weld Plate No.	Interpass / °C	Filler Metal	Plate Condition
Plate T50	50-70	CamAlloy 4	Constrained
Plate T200	190-210	CamAlloy 4	Constrained
Plate A50	50-70	Autorod 308LSi	Constrained

Metallographic and microhardness examination

A 10mm thick, cross sectional slice was taken from the centre of the weld, after the cross-weld cut for the contour method was made and the surface had been profiled. The cross sectional surface was ground flat and polished using standard metallographic techniques. The polished surface was electrolytically etched using Fry's reagent and imaged using optical microscopy. Because the base metal is anodic with respect to the weld, it was first covered with nail polish, which was removed using acetone after etching. The initial examinations showed the visible weld fusion region extended to 5mm outside the original weld groove in all directions.

Vickers hardness mapping was also carried out on the transverse section of the as welded plates with 1 mm by 2 mm grid spacing using an applied load of 2kg. Metallography and hardness measurements are only presented for martensitic welds (plate T50 and plate T200).

Neutron diffraction stress measurement

Residual stresses in each sample plate were first characterised, non destructively, by neutron diffraction method using the Engin-X beam line at the ISIS facility, Oxfordshire, UK. The lattice parameter variations in each of the phases were measured in three orthogonal directions using the "*time of flight*

method” with full Rietveld style refinement [19]. As a result of the dual-detector system employed at Engin-X, the three orthogonal directions could be obtained using 2 sample orientations. A set of 3mm radial collimators were employed to give a nominal gauge volume of 3x3x3mm [20]. When the sample was oriented such that the welding direction was vertical, the vertical slits were opened to 10mm to reduce counting times, but without reducing the spatial resolution in the normal and transverse directions. Strain was calculated using

$$\varepsilon = \frac{a^{xyz} - a_0^{xyz}}{a_0^{xyz}}, \quad (1)$$

where a^{xyz} is the refined lattice parameter at a particular gauge location (x, y, z) and $a_0^{x,y,z}$ is the lattice parameter corresponding to a stress-free condition at the sample location (x, y, z) . Stress-free samples were created using comb-like sample cut from a region towards the ends of the welded plates. The comb-like samples allowed stress free lattice parameter measurements at the same distances from the weld centre where the residual stresses are measured (i.e. each tooth on the comb-like sample corresponds to a certain gauge location) [21,22]. Given the size of each sample plate, cutting a thin comb-like sample from the end of each plate does not significantly alter the residual stress profile in the centre of the plates. Stress was calculated from the elastic strain measurements using

$$\sigma_{xx} = \frac{E((1-\nu)\varepsilon_{xx} + \nu(\varepsilon_{yy} + \varepsilon_{zz}))}{(1+\nu)(1-2\nu)}, \quad (2)$$

where σ_{ii} and ε_{ii} are the normal stress and strain respectively for the respective i -direction. In view of the fact that the whole diffraction profile is refined using a single crystal model, the response averages out the strain response for each diffraction peak, therefore the bulk Young’s modulus, E and Possion’s ratio, ν are employed rather than diffraction elastic constants that would be required for a single peak analysis [23].

Contour method of stress measurement

Upon completion of the neutron diffraction measurements, the plates were sectioned along the normal-transverse plane at the mid-point along the weld beads. The sectioning was performed using Wire-Electro-Discharge-Machining,

completed in a single pass using skim cut settings. During cutting the plates were kept clamped to the work table to prevent any rigid body movement.

The surface displacements were mapped using a Nano focus, Microscan, confocal laser profilometer. The data were cleaned and smoothed to remove outliers and noise and then fed into an FE model. The stress required to cause such surface displacements was determined and extracted across the surface of the cut to reveal the stress presented in the sample prior to sectioning.

The contour method can be affected by artefacts resulting from the cutting process [24,25]. These are often only significant in the first millimetre or so from a free surface. Because the bulk stresses close to the weld deposit (far from the plate edges) are our primary interest, no attempt was made to correct for the surface measurements and these data were removed from the calculation.

Finite element modelling

In this work, SYSWELD FE code [25] is used as it is one of a few specifically designed codes to include transformation plasticity (Greenwood and Johnson mechanism). A 2D model was built to investigate the effect of interpass temperature which was verified by some 3D modelling previously reported [18]. The mechanical properties of Camalloy 4 were determined as a function of temperature using an electro-thermo mechanical testing (ETMT) machine coupled with a digital image correlation (DIC) system for surface strain measurement. More details of the mechanical properties of the tested alloy can be found in [17,26].

Defining the thermal model

Each weld bead (pass) is considered to be deposited as a block (sometimes called block-dumping), with a thermal cycle imposed on the whole pass [27]. The heat power density function, as shown in eq. (3),

$$Q(x, y, z) = Q_f \exp \left(- \left(\frac{x^2}{a_f^2} + \frac{y^2}{b^2} + \frac{z^2}{c^2} \right) \right) \text{ for } x > 0 \quad (3)$$

$$Q(x, y, z) = Q_r \exp\left(-\left(\frac{x^2}{a_r^2} + \frac{y^2}{b^2} + \frac{z^2}{c^2}\right)\right) \text{ for } x < 0$$

is described mathematically by empirical parameters that need to be calibrated before the heat source can be applied. In all cases an arc efficiency of 0.8 was assumed for each welding pass. The calibration was carried out by seeking the best possible reproduction of the fusion zone (FZ) and heat affected zone (HAZ) in the first pass. The FZ/HAZ boundaries are normally estimated by plotting the maximum temperature envelope on a contour plot focusing on a contour value of 1500°C for the FZ and a minimum contour value of 850°C for the HAZ.

An averaged thermal cycle for the whole weld bead was then exported and compiled for the use of the multi-pass welding simulations. The welding speed for Pass 8 was 1.08 mm s⁻¹ compared to 1.3 mm s⁻¹ for all other passes. Consequently a different set of parameters were fitted for Pass 8 using a separate 2D transient welding analysis.

The thermal properties used in this work are given elsewhere [18]. The predicted 1500°C peak temperature contour corresponding to the fusion zone is compared with the macrostructure of the weld cross-section in Figure 2. Considerable weld dilution is observed in the fusion zone extending well beyond the foot print of the original groove, but still comparable with the optical micrographs.

In order to identify the optimum interpass hold temperature, four different interpass temperatures, 50, 100, 150 and 200°C, are modelled (denoted as Model T50, Model T100, Model T150 and Model T200).

Modelling the Martensitic Transformation

The extent of the martensite transformation can be described by the Koistinen-Marburger relationship [28]

$$X(T) = 1 - \exp(-b(M_s - T)), \quad \text{for } T < M_s, \quad (4)$$

where $M_s = 214^\circ\text{C}$ and b is a fit parameter ($= 0.014 \text{ K}^{-1}$ in this study).

The details of FE meshing used in the 2D analysis of multipass welding, is shown in Fig. 2c. The stainless 304L plate cannot transform throughout the entire welding process and it is assumed that the first bead stays mostly austenitic in all cases because of dilution. To model the dilution effect, a simple approximation is applied in which the initial phase of the first bead is assumed to be 50% austenitic plus 50% martensitic, while the second to the eighth beads are allowed to fully transform martensitically. If the amount of the retained austenite can be measured or accurately estimated, a better approximation could be made by calibrating the K-M coefficients M_s and b , or through the use of a progressive transition zone. Nevertheless, the current assumption should not affect our main focus on the effect of the interpass holding temperature of residual stresses.

Results

Vickers Microhardness

The hardness (HV2) maps are shown in Figure 3 from which the presence of martensitic weld metal is evident for both plates T50 and T200 from the high hardness values (>250 HV2) compared to that of the parent austenitic regions (<200 HV2). It is also observed that the hardness of the first weld bead of both tested plates is between of 200-250 HV2 similar to the hardness obtained in the heat affected zone (HAZ) for both plates suggesting the microstructure of the first bead is significantly austenitic rather than 100% martensitic. It is also evident that the hardness plateau of the HAZ for the higher interpass temperature (200°C) is wider than for the lower interpass temperature (50°C).

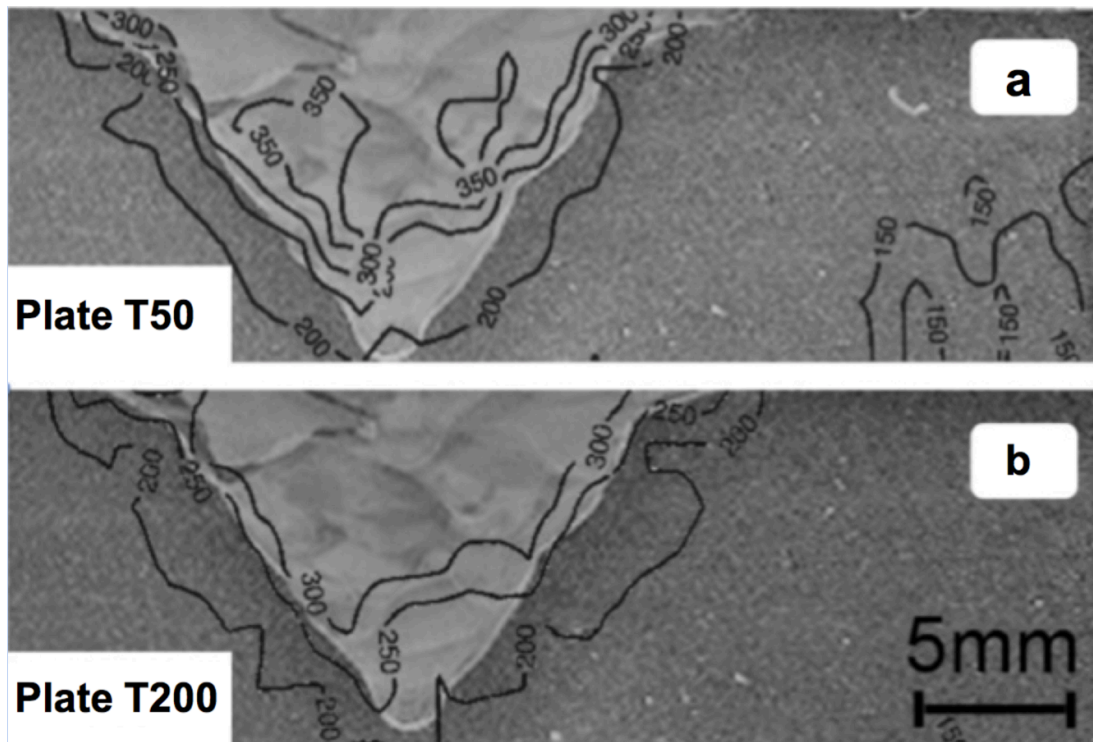


Figure 3: a) and b) are weld microstructures with superimposed microhardness maps (in HV2) for the plate T50 (50°C interpass temperature) and plate T200 (200°C interpass temperature) respectively.

For the plate welded using a 200°C interpass temperature (plate T200), the result shows that except for the first weld bead, there is no major variation in the hardness values of the different passes. However, for plate T50, a higher hardness was obtained in the central passes (beads 2, 3, 4 and 5). This is presumably due to accumulated plastic strain in the martensite caused by subsequent passes, although further work would be required to investigate this relationship as anneal may be expected as a result of subsequent heating cycles.

Phase fraction

The variation in phase fraction of martensite measured at the weld centreline is presented in Figure 4. These results are calculated using ASTM standard for retained austenite determination from the neutron diffraction profiles. As expected no martensite is observed for the non-transforming austenitic filler (Aurorod OK 308LSi) nor towards the bottom (~8mm) of the plates. This is despite the presence of the fusion zone extending beyond this location.

Martensite is first detected in the neutron measurements with the gauge centre 10mm from the top surface, steadily increasing to a maximum of 70-80% 6mm

from the top surface. These results broadly agree with the hardness maps and are within the tolerance of the assumptions made for the FE modelling.

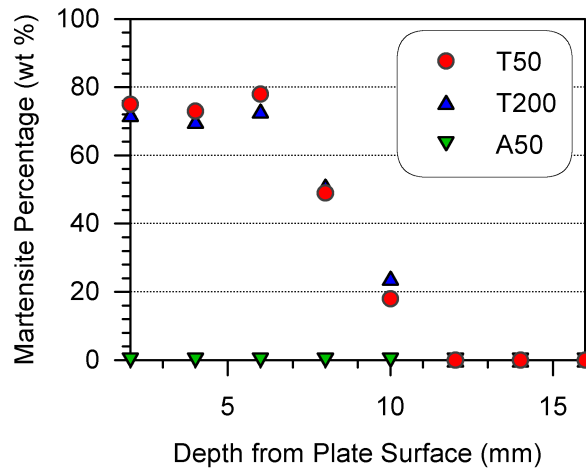


Figure 4: Variation in martensite fraction from top surface to weld root as determined by neutron diffraction.

Residual stress measurements

The residual stresses, measured by neutron diffraction in the longitudinal and transverse directions, are shown in Figure 5 (versus depth) and Figure 6 (versus lateral distance from the weld centreline). For both welds made with the transforming filler material (Camalloy4), significant regions of compressive stress are observed in the weld zone. Unsurprisingly, the stresses in the longitudinal direction are of the greatest magnitude. For the austenitic weld, the residual stress is largest at the weld centre reaching around +400MPa. By contrast the stress in the weld zone for the LTT weld filler is largely compressive reaching a peak of about -600MPa when using the higher interpass temperature (T200). For the weld with the lower interpass temperature (plate T50), significant compressive stresses are only observed for the later passes while tensile stresses similar to those in the austenitic weld are seen for the earlier passes (~+400MPa). In the HAZ, both to the side and below the fusion zone, the stresses are similar to those for the austenitic weld. The contour measurements, conducted at the same locations as of the neutron diffraction measurements, show values of longitudinal residual stress (see Figure 5 & 6) that are in very good agreement with the neutron diffraction scans.

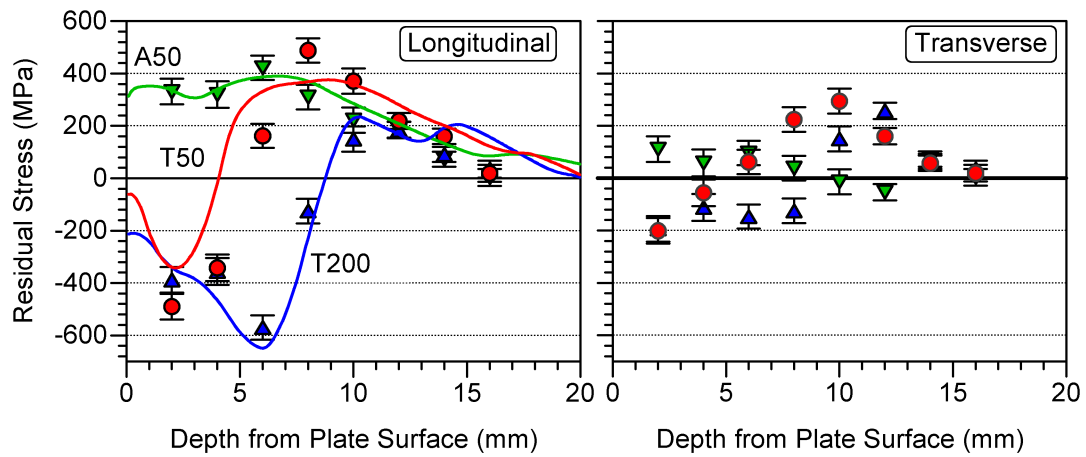


Figure 5: a) Longitudinal and b) transverse residual stress profiles with depth through the thickness of the plates at the weld-centreline. The markers denote neutron diffraction measurements while in LHS the corresponding continuous lines denote the contour method results for the same plate.

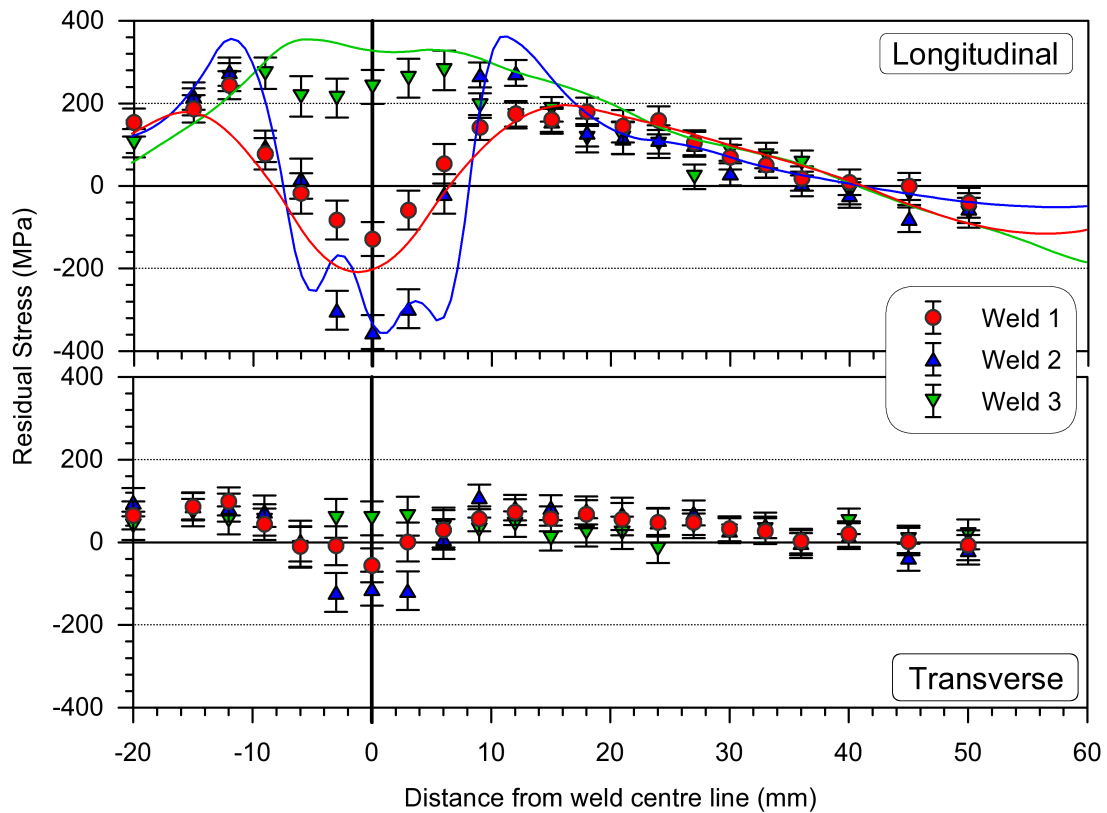


Figure 6: Longitudinal (top) and transverse (bottom) residual stress profiles as a function of distance from the weld centrelines at a depth of 4mm below the plate surface. Markers denote neutron diffraction measurements and the corresponding solid lines denote the contour method results for the same plate.

Full contour maps of longitudinal residual stress across the entire normal-transverse plane, calculated from contour method measurements are plotted in Figure 7 for the three plates. These confirm that the compressive stress in plate T200 extends across the majority of the fusion zone, whereas for plate T50 this is

confined to the last 3 passes only. In addition, these contour maps reveal that despite the large regions of compressive stress, regions of high tensile stress are present in the HAZ for plate T200 and in the HAZ and fusion zone of plate T50. These tensile stresses are of greater magnitude than those found in plate A50, albeit over smaller regions. It should also be noted that tensile stresses are observed in the bottom corners of the plates. These arise from the tack welds used to attach the plates to the welding table.

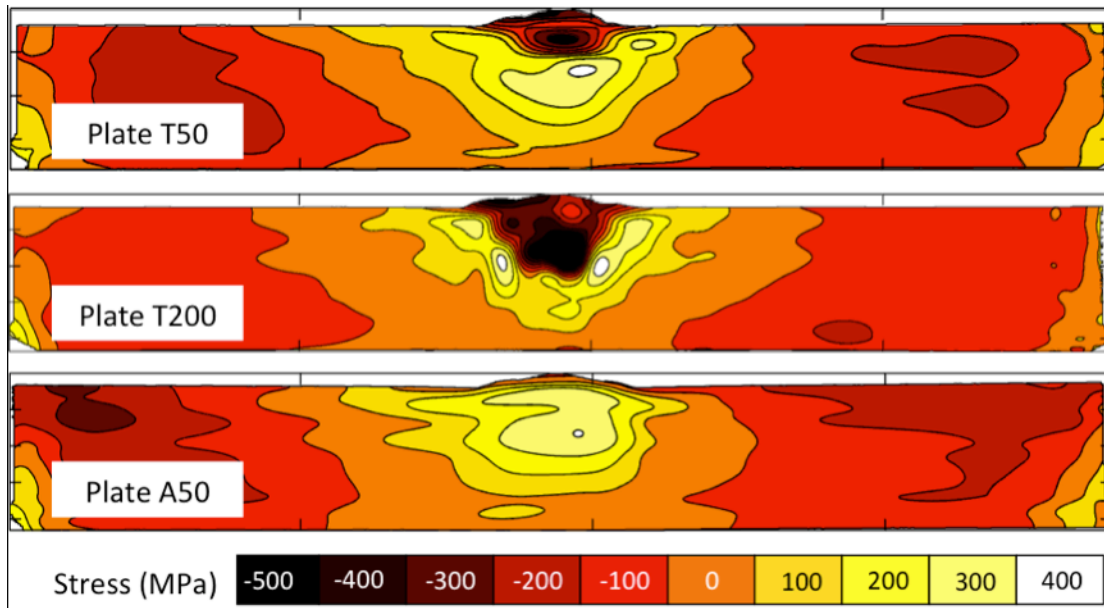


Figure 7: Maps of longitudinal residual stress calculated using the contour method for plates T50, T200 (both Camalloy 4) and A50 (308L).

Discussion

In order to rationalise the measurements it is useful to consider the FE predictions, which enable us to examine the temporal and spatial variation in the extent of the transformation (Figure 8) From the FE predictions, it is evident that for the low interpass temperature model (T50) the weld filler transforms to around 50% martensite as it is laid down. The percentage of martensite remains almost constant as more layers are deposited. However, after the final (8th) pass the weld is cooled to room temperature causing further transformation such that the final martensite fraction is around 70%. The martensite fraction predicted by the FE model is in good accordance with the phase fraction determined experimentally (Figure 4).

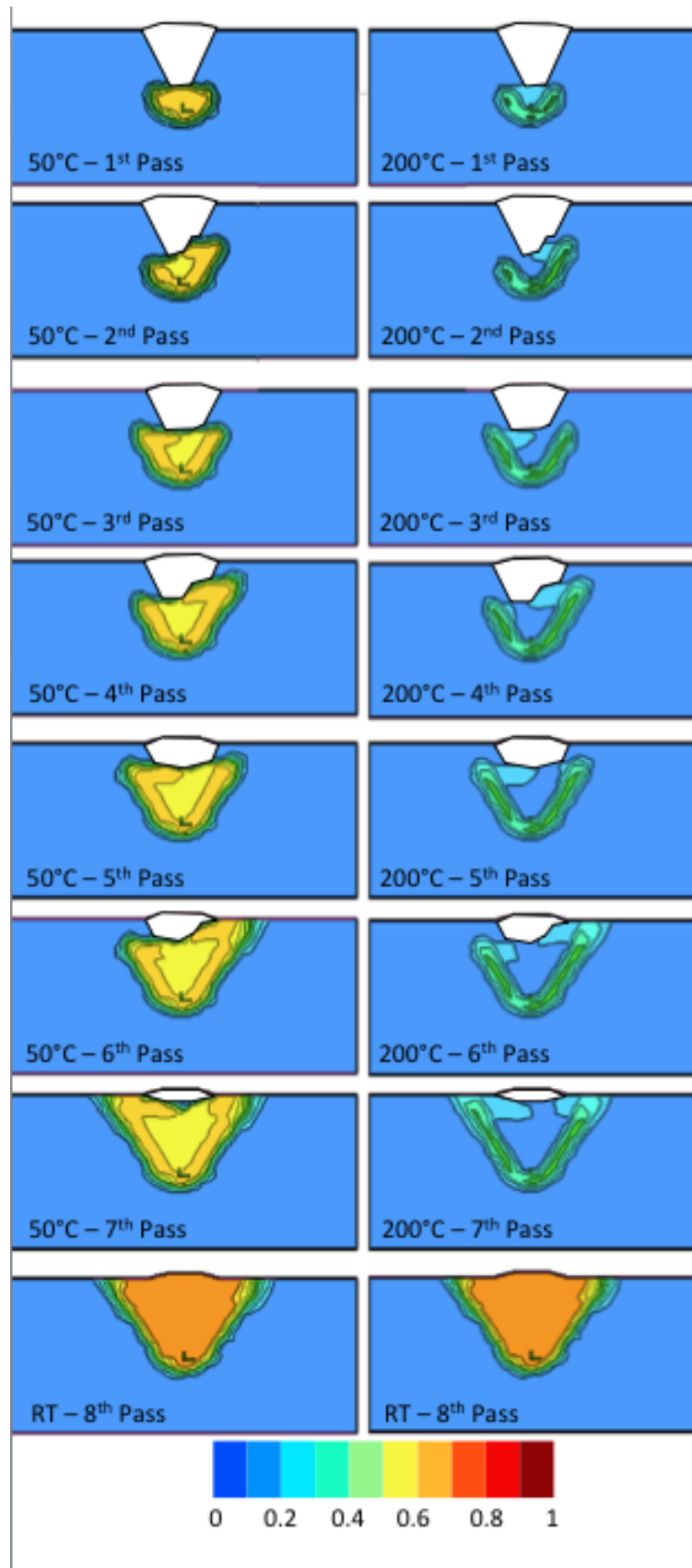


Figure 8: The predicted martensite fraction for after the laying down of each pass for interpass hold temperatures of 50°C (left) and 200°C (right) . After the 8th pass the plate has been allowed to cool to room temperature.

By contrast the elevated holding temperature between weld passes (model T200) prevents significant transformation from taking place during the welding procedure. Consequently, only around 40% martensite forms near the boundary with the base plate and almost no transformation is predicted to occur in the beads laid down away from the base plate. It should also be noted that dilution may decrease the level of transformation observed near the sides of the original groove. As a result in this case, most of the transformation is predicted to occur upon final cooling of the weld, giving approximately the same fractions of martensite (~70%) as for the lower interpass temperature weld.

The observed differences are reflected in the final residual stresses as a function of interpass temperature shown in Figure 9. Whatever the interpass temperature, there is a compressive residual stress zone towards the top of the fusion zone associated with the martensitic transformation of the final passes. Similarly in all cases the stresses in the parent metal beneath the weld are tensile just below the groove falling almost to zero towards the underside of the plate. Similarly in all cases the base plate far from the weld is in low level tension. Consequently, the major differences lie in the region where the early weld beads are laid down. As the interpass temperature is lowered the compressive stress in this region is lost.

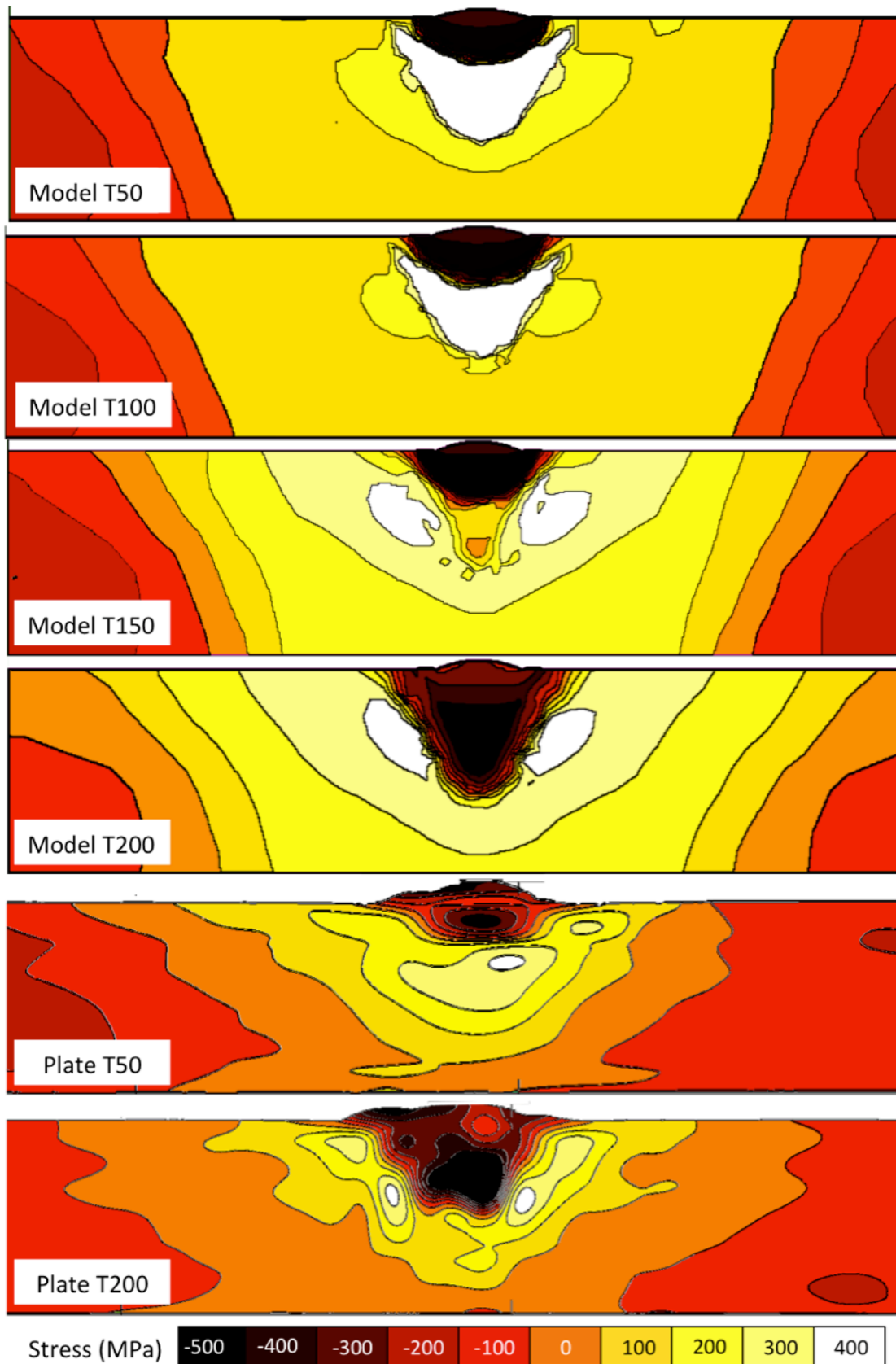


Figure 9: Predicted longitudinal residual stresses for 4 interpass temperatures plotted alongside measured longitudinal stresses for plate T50 and T200 using the same stress contours levels.

This effect can be seen even more clearly in the line profiles shown in Figure 10. Indeed, the FE predicts a higher magnitude of tensile stress in the lower part of the weld groove ($\sim 1000\text{MPa}$) than is measured ($\sim 400\text{MPa}$). By contrast the magnitudes of residual stress predicted for the model T200 case is in good agreement with the measurements for plate T200.

It is noteworthy that for both the models and the experimental plates the stresses in the last few beads are the same independent of interpass temperature.

The over prediction of tensile residual stress in the region where the early beads were laid down is clear from Figure 10. Further work is required to identify the source of the inconstancy in predicted and measured tensile residual stress. . Clearly a number of factors need to be taken into account including annealing effect of subsequent passes as well as the effect of transformation plasticity and the work hardenability of this zone.

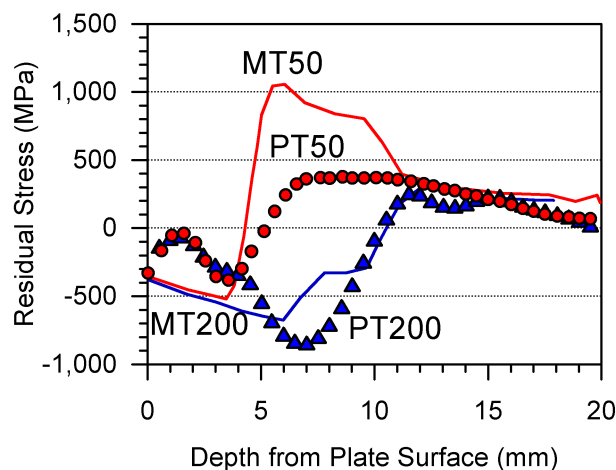


Figure 10: Predicted longitudinal residual stresses (continuous lines) plotted alongside the contour method measurements for similar conditions (modelled data denoted M and contour data denoted P) adapted from [18].

Nevertheless, the simulations do indicate that a temperature around 200°C is necessary if the transformation strain, accompanying the martensitic transformation, is to be exploited to generate compressive weld stresses throughout the whole multipass weldment. This is in agreement with [9,15] where maintaining an interpass temperature in excess of the M_s has shown to achieve bulk compressive residual stresses.

Another important effect is the dilution which is evident from Figure 2. In the model the composition of the 1st bead has been assumed to be 50% austenitic plus 50% martensitic to account for dilution. For the T200 case, some further studies on the effect of dilution have been carried out by modifying the untransformed and transformed phase fractions and the results are plotted in Figure 11. It can be seen that the compressive zone is predicted to move from the bottom of the 1st bead toward the 2nd bead when the level of retained austenite increases. This is not surprising since transformation plasticity cannot occur without the martensite phase transformation leading to higher tensile residual stresses there. It is thus very important to accurately measure or estimate the retained austenite in the weld. If the retained austenite cannot be controlled below a certain level ($\sim 70\%$ in our case) a significant increase in the tensile zone should be expected.

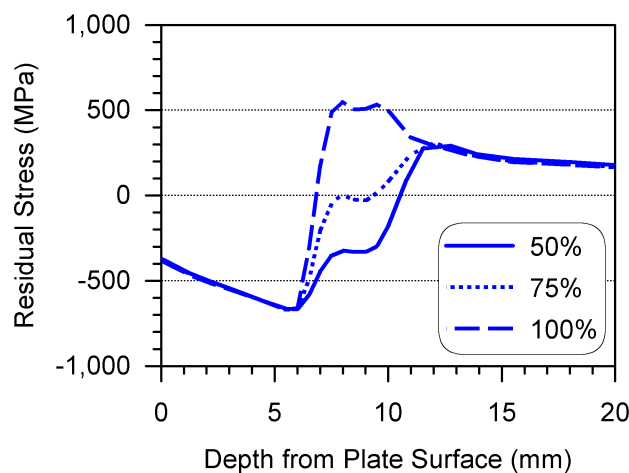


Figure 11: Effect of final austenite fraction on the predicted stress when the interpass temperature is kept at 200°C adapted from [18].

Conclusions

In this study three weld samples have been produced, two using the novel filler material, Camalloy 4 but with different interpass temperatures ($\sim 50^\circ\text{C}$ and $\sim 200^\circ\text{C}$) and the third weld was a benchmark sample made using a non-transforming austenitic weld filler with an interpass temperature of $\sim 50^\circ\text{C}$. As expected, the stress field in the non-transforming weld filler is tensile everywhere reaching a peak stress of around $\sim +400\text{MPa}$. For the low transformation temperature filler, 70% transformation to martensite was

measured throughout the weld zone irrespective of the interpass hold temperature. The final residual stresses however were found to be heavily dependent on the interpass temperature. The simulations suggest that the interpass hold temperature needs to be around 200°C in order to delay the phase transformation of the deposited layers until the whole welding sequence is complete (i.e. ideally all layers should be cooled below the martensite start temperature and transform to martensite in the same time). In this case the whole weld zone is placed in residual compression reaching around -600MPa in the centre of the weld zone. With a 50°C interpass temperature most of the transformation occurs immediately as the bead is laid down. The stresses in the HAZ are slightly more tensile than arise when non-transforming filler or a lower interpass temperature are employed.

While this study has used an LTT filler with a transformation and a transformation temperature such that significant compressive residual stresses are generated, in principle it would also be possible to design an LTT filler such that the weld stresses are approximately zero according to the structural integrity requirements in a given application.

The modelled tensile stresses appear to be much larger in the early weld passes than are measured in practice – this difference will be the focus of further study. Nevertheless this study shows that the interpass hold temperature needs to be carefully selected for low transformation temperature weld fillers if they are to mitigate tensile weld stresses in the same manner as had been demonstrated previously for single pass welds.

Acknowledgements

The funding of EPSRC through grants GR/S62840/01 and GR/S62857/01 is acknowledged. Complementary funding as well as help with the welding is gratefully acknowledged from Rolls-Royce plc along with helpful suggestions from Dr Paul Hurrell regarding the use of interpass hold temperature.

- [1] P.J. Withers, Residual stress and its role in failure, *Reports Prog. Phys.* 70 (2007) 2211–2264. doi:10.1088/0034-4885/70/12/R04.
- [2] J. a. Francis, H.K.D.H. Bhadeshia, P.J. Withers, Welding residual stresses in ferritic power plant steels, *Mater. Sci. Technol.* 23 (2007) 1009–1020. doi:10.1179/174328407X213116.
- [3] M. Turski, P.J. Bouchard, a. Steuwer, P.J. Withers, Residual stress driven creep cracking in AISI Type 316 stainless steel, *Acta Mater.* 56 (2008) 3598–3612. doi:10.1016/j.actamat.2008.03.045.
- [4] W. Wang, L. Huo, Y. Zhang, D. Wang, H. Jing, New developed welding electrode for improving the fatigue strength of welded joints, *J. Mater. Sci. Technol.* 18 (2002) 527–531.
- [5] A. Ohta, N. Suzuki, Y. Maeda, K. Hiraoka, T. Nakamura, Superior fatigue crack growth properties in newly developed weld metal, *Int. J. Fatigue.* 21 (1999) 113–118. doi:10.1016/S0142-1123(99)00062-6.
- [6] A.A. Shirzadi, H.K.D.H. Bhadeshia, L. Karlsson, P.J. Withers, Stainless steel weld metal designed to mitigate residual stresses, *Sci. Technol. Weld. Join.* 14 (2009) 559–565. doi:10.1179/136217109X437178.
- [7] J.A. Francis, H.J. Stone, S. Kundu, R.B. Rogge, H.K.D.H. Bhadeshia, P.J. Withers, Transformation Temperatures and Welding Residual Stresses in Ferritic Steels, *ASME Press. Vessel. Pip.* (2007) 949–956. doi:10.1115/PVP2007-26544.
- [8] T.I. Ramjaun, H.J. Stone, L. Karlsson, M.A. Gharghour, K. Dalaei, R.J. Moat, H.K. Bhadeshia, Surface residual stresses in multipass welds produced using low transformation temperature filler alloys, *Sci. Technol. Weld. Join.* 19 (2014). doi:10.1179/1362171814Y.0000000234.
- [9] T. Ramjaun, H.J. Stone, L. Karlsson, J. Kelleher, R.J. Moat, J.R. Kornmeier, K. Dalaei, H.K.D.H. Bhadeshia, Effect of interpass temperature on residual stresses in multipass welds produced using low transformation temperature filler alloy, *Sci. Technol. Weld. Join.* 19 (2014).

- doi:10.1179/1362171813Y.0000000162.
- [10] H. Dai, J.A. Francis, H.J. Stone, H.K.D.H. Bhadeshia, P.J. Withers, Characterizing phase transformations and their effects on ferritic weld residual stresses with X-rays and neutrons, in: *Metall. Mater. Trans. A Phys. Metall. Mater. Sci.*, 2008: pp. 3070–3078. doi:10.1007/s11661-008-9616-0.
- [11] H. Murakawa, M. Béreš, C.M. Davies, S. Rashed, A. Vega, M. Tsunori, K.M. Nikbin, D. Dye, Effect of low transformation temperature weld filler metal on welding residual stress, *Sci. Technol. Weld. Join.* 15 (2010) 393–399. doi:10.1179/136217110X12714217309614.
- [12] R.J. Moat, H.J. Stone, A. A. Shirzadi, J. A. Francis, S. Kundu, A. F. Mark, H.K.D.H. Bhadeshia, L. Karlsson, P.J. Withers, Design of weld fillers for mitigation of residual stresses in ferritic and austenitic steel welds, *Sci. Technol. Weld. Join.* 16 (2011) 279–284. doi:10.1179/1362171811Y.0000000003.
- [13] D. Thibault, P. Bocher, M. Thomas, M. Gharghoury, M. Côté, Residual stress characterization in low transformation temperature 13%Cr-4%Ni stainless steel weld by neutron diffraction and the contour method, *Mater. Sci. Eng. A.* 527 (2010) 6205–6210. doi:10.1016/j.msea.2010.06.035.
- [14] J. Dixneit, A. Kromm, A. Hannemann, P. Friedersdorf, T. Kannengiesser, J. Gibmeier, In-situ load analysis in multi-run welding using LTT filler materials, *Weld. World.* 60 (2016) 1159–1168. doi:10.1007/s40194-016-0373-1.
- [15] J. Dixneit, A. Kromm, M. Boin, R.C. Wimpory, T. Kannengiesser, J. Gibmeier, D. Schroepfer, Residual stresses of LTT welds in large-scale components, *Weld. World.* 61 (2017) 1089–1097. doi:10.1007/s40194-017-0502-5.
- [16] T.I. Ramjaun, H.J. Stone, L. Karlsson, J. Kelleher, S.W. Ooi, K. Dalaei, J. Rebelo Kornmeier, H.K.D.H. Bhadeshia, Effects of dilution and baseplate strength on stress distributions in multipass welds deposited using low transformation temperature filler alloys, *Sci. Technol. Weld. Join.* 0 (2014) 1362171814Y.000. doi:10.1179/1362171814Y.0000000209.

- [17] H. Dai, A.F. Mark, R.J. Moat, A.A. Shirzadi, H.K.D.H. Bhadeshia, L. Karlsson, P.J. Withers, Modelling of Residual Stress Minimization through Martensitic Transformation in Stainless Steel Welds, GRAZ, Austria., in: 9th Int. Semin. Numer. Anal. Weldability, Graz, 2009: pp. 239–252.
- [18] H. Dai, R.J. Moat, P.J. Withers, Modelling the interpass temperature effect on residual stress in low transformation temperature stainless steel welds, in: Am. Soc. Mech. Eng. Press. Vessel. Pip. Div. PVP, 2011. doi:10.1115/PVP2011-57329.
- [19] P.J. Withers, Mapping residual and internal stress in materials by neutron diffraction, *Comptes Rendus Phys.* 8 (2007) 806–820. doi:10.1016/j.crhy.2007.09.015.
- [20] P.J. Withers, M.W. Johnson, J.S. Wright, Neutron strain scanning using a radially collimated diffracted beam, *Phys. B Condens. Matter.* 292 (2000) 273–285. doi:10.1016/S0921-4526(00)00481-6.
- [21] P.J. Withers, M. Preuss, A. Steuwer, J.W.L. Pang, Methods for obtaining the strain-free lattice parameter when using diffraction to determine residual stress, *J. Appl. Crystallogr.* 40 (2007) 891–904. doi:10.1107/S0021889807030269.
- [22] D.J. Hughes, M.N.J.D.G. Hattingh, P.J. Webster, The Use of Combs for Evaluation of Strain-free References for Residual Strain Measurements by Neutron and Synchrotron X-ray Diffraction, *J. Neutron Res.* 11 (2003) 289–293. doi:10.1080/10238160410001726765.
- [23] M.R. Daymond, M. a. M. Bourke, R.B. Von Dreele, B. Clausen, T. Lorentzen, Use of Rietveld refinement for elastic macrostrain determination and for evaluation of plastic strain history from diffraction spectra, *J. Appl. Phys.* 82 (1997) 1554. doi:10.1063/1.365956.
- [24] M.B. Prime, A.T. DeWald, The Contour Method, in: *Pract. Residual Stress Meas. Methods*, 2013: pp. 109–138. doi:10.1002/9781118402832.ch5.
- [25] M.B. Prime, M.R. Hill, A. DeWald, R.J. Sebring, V.R. Dave, M.J. Cola, Residual stress mapping in welds using the contour method, *Trends Weld. Res. Proc.* 836 (2002) 891–896. doi:10.4028/www.scientific.net/MSF.490-

491.294.

- [26] A.F. Mark, R. Moat, A. Forsey, H. Abdolvand, P.J. Withers, A new method for quantifying anisotropic martensitic transformation strains accumulated during constrained cooling, *Mater. Sci. Eng. A.* 611 (2014). doi:10.1016/j.msea.2014.06.012.
- [27] C.D. Elcoate, R.J. Dennis, P.J. Bouchard, M.C. Smith, Three dimensional multi-pass repair weld simulations, *Int. J. Press. Vessel. Pip.* 82 (2005) 244–257. doi:10.1016/j.ijpvp.2004.08.003.
- [28] J.A. Francis, H.J. Stone, S. Kundu, H. Bhadeshia, R.B. Rogge, P.J. Withers, L. Karlsson, The Effects of Filler Metal Transformation Temperature on Residual Stresses in a High Strength Steel Weld, *J. Press. Vessel Technol. Asme.* 131 (2009) 8. doi:10.1115/1.3122036.